# *Primary Resistance Mechanism of the Canine Distemper Virus Fusion Protein against a Small-Molecule Membrane Fusion Inhibitor*

**David Kalbermatter[1#], Neeta Shrestha[2#], Nadine Ader-Ebert[3#], Michael Herren[2], Pascal Moll[2], Richard K. Plemper[4], Karl-Heinz Altmann[5], Johannes P. Langedijk[6], Flavio Gall[7], Urs Lindenmann[7], Rainer Riedl[7], Dimitrios Fotiadis[1] and Philippe Plattet[2*]**

[1] Institute of Biochemistry and Molecular Medicine, and Swiss National Centre of Competence in Research (NCCR) TransCure, University of Bern, CH-3012 Bern, Switzerland.

[2] Division of Experimental and Clinical Research, Vetsuisse Faculty, University of Bern, CH-3001 Bern, Switzerland.

[3] Institute of Virology and Immunology, Bern and Mittelhäusern, Switzerland

[4] Institute for Biomedical Sciences, Georgia State University, Atlanta, GA, USA

[5] Institute of Pharmaceutical Sciences, Department of Chemistry and Applied Biosciences, ETH Zurich, Zurich, Switzerland

[6] Janssen Infectious Diseases and Vaccines, Leiden, Netherlands

[7] Institute of Chemistry and Biotechnology, Center for Organic and Medicinal Chemistry, Zurich University of Applied Sciences (ZHAW), Einsiedlerstrasse 31, CH-8820 Wädenswil, Switzerland

# contributed equally to this work

* To whom correspondence should be addressed, Bremgartenstrasse 109a, 3001 Bern, Switzerland. Phone: +4131 631 23 70. Fax: +4131 631 25 38.
E-mail: philippe.plattet@vetsuisse.unibe.ch

Abstract: 237
Text: 5348
Running Title: 3G-dependent prefusion CDV F stabilization
Keywords: fusion inhibitors, fusion protein, head-stalk interface, Morbillivirus cell entry, prefusion state stabilization

## ABSTRACT

Morbilliviruses (*e.g.* measles virus [MeV] or canine distemper virus [CDV]) employ the attachment (H) and fusion (F) envelope glycoproteins for cell entry. H protein engagement to a cognate receptor eventually leads to F-triggering. Upon activation, F proteins transit from a prefusion to a postfusion conformation; a refolding process that is associated with membrane merging. Small-molecule morbilliviral fusion inhibitors such as the compound 3G (a chemical analog in the AS-48 class) were previously generated and mechanistic studies revealed a stabilizing effect on morbilliviral prefusion F trimers. Here, we aimed at designing 3G-resistant CDV F mutants by introducing single cysteine residues at hydrophobic core positions of the helical stalk region. Covalently-linked F dimers were generated, which highlighted substantial conformational flexibility within the stalk to achieve those irregular F conformations. Our findings demonstrate that “top-stalk” CDV F cysteine mutants (F-V571C and F-L575C) remained functional and gained resistance to 3G. Conversely, although not all “bottom-stalk” F cysteine variants preserved proper bioactivity, those that remained functional exhibited 3G-sensitivity. According to the recently determined prefusion MeV F trimer/AS-48 co-crystal structure, CDV residues F-V571 and F-L575 may directly interact with 3G. A combination of conformation-specific anti-F antibodies and low-resolution electron microscopy structural analyses confirmed that 3G lost its stabilizing effect on “top-stalk” F cysteine mutants thus suggesting a primary resistance mechanism. Overall, our data suggest that the fusion inhibitor 3G stabilizes prefusion CDV F trimers by docking at the top of the stalk domain.

## 1. Introduction

Measles is a vaccine preventable human disease caused by the measles virus (MeV). MeV is an enveloped RNA virus which belongs to the genus *Morbillivirus* in the family *Paramyxoviridae* and is considered one of the most contagious infectious pathogens worldwide (Lamb and Parks, 2007). However, due to suboptimal vaccine delivery in developing countries and increasing cases of vaccination refusals in industrialized areas, MeV continues to kill around 90'000 people per year (Simons et al., 2012). The related canine distemper virus (CDV) exhibits high potential to easily cross the species barriers and was recently associated with severe outbreaks in monkeys (Sakai et al., 2013). Consistent with this zoonotic capability, CDV also represents an important threat for endangered animal populations, such as giant pandas in China (Feng et al., 2016; Jin et al., 2017). Although effective antivirals may support vaccination campaigns and help to contain local epidemics, no FDA-approved anti-morbilliviral drug is currently available. However, efficacy of a small-molecule inhibitor of the viral polymerase was recently demonstrated in a large animal model of morbillivirus-mediated pathogenesis (ferrets) when orally administrated at the onset of viremia (post-exposure treatment protocol) (Krumm et al., 2014). A peptidic fusion inhibitor was also shown to protect against lethal MeV infections in a cotton rats model, even though, in that case, prophylactic protocols with intranasal delivery of the antiviral were required, which certainly challenge clinical feasibility (Mathieu et al., 2015).

The morbilliviral cell entry system may define another attractive target for antiviral drug development. Indeed, in both viruses only one serotype has been described, thereby highlighting the lack of sufficient plasticity within the two surface glycoproteins to efficiently escape binding of neutralizing antibodies. Importantly, structural and mechanistic understanding of the molecular mechanism of cell entry is supportive to successfully achieve the rationale design and chemical improvements of desired inhibitors.

MeV and CDV cell entry is mediated by the co-operated action of the two tightly interacting attachment (H) and fusion (F) envelope glycoproteins. Upon H-to-receptor binding, a cascade of conformational changes occurs, which in turn translates into F activation at the right time and place (Ader-Ebert et al., 2015; Ader et al., 2012; Apte-Sengupta et al., 2013; Brindley et al., 2012; Herren et al., 2018; Navaratnarajah et al., 2014; Navaratnarajah et al., 2012; Plattet et al., 2016). This mechanism is thought to lead to the merging of the viral envelope with the host cell plasma membrane, which is followed by the formation of a fusion pore and, ultimately, allowing the injection of the genetic information into the cytosol (Lamb and Parks, 2007; Russell et al., 2001).

The F protein of morbilliviruses belongs to class I viral fusion proteins, such as Ebola virus GP, human immunodeficiency virus GP160 or influenza virus HA. The F protein is first synthesized as a long inactive precursor called F0. During its transport to the cellular surface,

F0 trimerizes and is further cleaved into two covalently-linked subunits F1 and F2. F1 is composed of an N-terminal hydrophobic fusion peptide, two heptad repeat regions (HRA and HRB), a long intervening sequence (between both HR domains) potentially encompassing the H-binding site, a transmembrane domain and a C-terminal cytoplasmic tail (Plattet et al., 2016). Based on the recently determined MeV F protein structure as well as reported crystal structures of related paramyxovirus and pneumovirus F proteins, it is assumed that F initially assumes a metastable, prefusion state (Hashiguchi et al., 2018; McLellan et al., 2013; Wong et al., 2016; Xu et al., 2015; Yin et al., 2006). The ectodomain contains a short stalk (mainly formed by the assembly of three HRB domains) and a large globular head, which has been subdivided into three subdomains (DI, DII and DIII). DIII mainly contains the three HRA regions, which fold compactly at the top of the head, whereas DI and DII constitute the base of the globular head (Yin et al., 2006). It is assumed that upon H-mediated F-triggering, the HRB helical bundle (stalk) unwinds, which in turn enables HRA regions to refold into a long trimeric coiled-coil and to thereby propel the fusion peptides towards the target cell membrane. The achieved F-conformational state is referred to as the pre-hairpin intermediate. Then, it is proposed that the three HRB regions swing around the base of the head and zipper-up along the central coiled-coil HRA to generate a highly stable six-helix bundle (6HB) structure (Plattet et al., 2016).

Although the formation of the 6HB is considered to correlate with membrane merging, assembly of a four or five-helix bundle may in fact be sufficient to drive spontaneous lipid mixing. Indeed, insertion of single cysteine substitution at the most membrane-proximal hydrophobic positions of the MeV F-HRB (stalk) region translated into the assembly of covalently-linked F-dimers with only moderate impact on membrane fusion activity. Because the cysteine mutation was introduced into each protomer, we speculated that dimer-of-trimers were generated (Brindley et al., 2014). Such hexameric structures may have involved two covalently-linked protomers from the same trimer and two covalently-linked protomers from two adjacent trimers (to balance the stoichiometry of covalent bonds and enable the assembly of productive prefusion-like hexameric structures). Importantly, strong evidence was provided to exclude temporary opening of the engineered disulfide bonds to achieve membrane fusion activity (Brindley et al., 2014).

AS-48 and derivative chemical analogs (*e.g.* 3G) represent a unique class of small-molecule morbilliviral fusion inhibitors with broad-spectrum activities, but with only moderate efficacy (low-to-sub micromolar range of 50% inhibitory concentrations) (Plemper et al., 2004; Singethan et al., 2010; Sun et al., 2006). It was previously demonstrated that those compounds potentially stabilized the prefusion state of MeV and CDV F proteins in turn preventing productive H-mediated F-activation (Avila et al., 2014; Doyle et al., 2006). The prefusion MeV F structure in complex with AS-48 strongly supported a mechanism of

inhibition through prefusion F stabilization by the compound. Indeed, AS-48 docks onto three hydrophobic pockets locating at the interface between the stalk and head regions (Hashiguchi et al., 2018); a microdomain that is likely critical for F activation since AS-48-resitance mutations mapped within or around the pocket and displayed either hyperfusogenic profiles or even turned dependent of AS-48 for their bioactivity (Doyle et al., 2006; Ha et al., 2017; Jurgens et al., 2015; Watanabe et al., 2015; Watanabe et al., 2013).

In this study, we aimed at investigating whether the engineering of disulfide bonds at core hydrophobic positions within the CDV F-stalk region would result in 3G-resitance profiles. Based on the usage of a cell-to-cell fusion assay, conformation specific anti-F monoclonal antibodies and low-resolution electron microscopy structural analyses, our data were suggestive for a primary resistance mechanism mediated by “top-stalk” CDV F cysteine mutants. These findings highlighted the important role of four CDV F residues (I564, V571, G572 and L575), all locating at the interface between the head and stalk domain, as essential amino acids potentially controlling the interaction with the fusion inhibitor 3G.

## 2. Materials and Methods

**2.1. Cell cultures and transfections.** Depending on the experiments, the cells used included Vero cells (ATCC CCL-81) or Vero cells stably expressing canine SLAM (Vero-cSLAM, kindly provided by Yusuke Yanagi, Kyushu University, Japan). Both cell type were grown in Dulbecco's modified Eagle medium (Gibco, Invitrogen) containing 10% fetal calf serum (FCS; BioSwissTech) and 1% penicillin-streptomycin at 37°C and 5% $CO_2$. The cells were transfected with TransIT-LT1 (Mirus) following the manufacturer's instructions. For regular cell-cell fusion assays, the extent of fusion induction was recorded by taking pictures of representative fields of view 24 hours post-transfection. In the indicated experiments, F and H-expressing Vero-cSLAM cells were treated, 24 hours post-transfection, with 50 mM of dithiothreitol (DTT) during 30 min, to potentially reactive fusion activity.

**2.2. Construction of expression plasmids.** All mutant CDV F protein-expressing plasmids are based on the pCI plasmid containing a modified version of CDV-F of the A75/17 CDV strain (Plattet et al., 2007; Plattet et al., 2005). Mutations in the CDV F-expressing DNA plasmid were introduced using the QuikChange lightning site-directed mutagenesis kit (Agilent Technologies). Furthermore, all F proteins contained a FLAG-tag inserted within the ectodomain (Ader et al., 2013).

**2.3. Quantitative fusion assay.** Vero cells in a 24-well plate were transfected with 0.5µg of H protein plasmid, 1µg of variant F protein plasmid and 1µg of the second part of the dual-split reporter plasmid (DPS 8-11) per well. At the same time Vero-cSLAM cells in a 24-well plate were transfected with 1µg DSP1-7. 24h post transfection the Vero cells expressing the fusion machinery and DPS 8-11 were detached with 80µl trypsin before adding 235µl DMEM (with or without the fusion inhibitor 3G) and transferring wells into individual tubes. Vero-cSLAM cells were detached with 80µl Trypsin before adding 235µl of DMEM (with or without the fusion inhibitor 3G) containing 120µM EnduRen™ Live Cell Substrate (Promega) and pooling these Vero-cSLAM. 300µl Vero-cSLAM cells were then distributed to the tubes containing the Vero cells. The mixed cells were distributed into four wells of a white 96-well plate per mutant. The plate was centrifuged 5min at 200g and then placed in the Cytation 5 Cell Imaging Multi-Mode Reader (BioTek). To quantify the luminescence intensity read-out, the maximum reached during the measurement was divided by the time to reach the maximum for every mutant. Thereby an indication of kinetics was gained.

**2.4. Immunofluorescence staining and flow cytometry.** Vero cells were transfected with 1 µg of various F-expressing DNA plasmids. One day post transfection, unfixed and unpermeabilized cells were washed twice with cold phosphate buffered saline (PBS) and

subsequently stained with the various antibodies (1:1000) for 1 hour at 4°C. The anti-CDV F mAbs 4941 and 3633 or anti-FLAG mAb (Sigma Aldrich) were employed. This was followed by washes with cold PBS and incubation of the cells with Alexa-fluor 488-conjugated secondary antibody (1:500) for 1 hour at 4°C. Cells were subsequently washed 2 times with cold PBS and consequently detached from the wells by adding PBS-EDTA (50 µM) 20 min at 37°C. The mean fluorescence intensity (MFI) of 10'000 cells was then measured by using a BD LSRII flow cytometer (Becton Dickinson). When indicated, brief heat shocks (5 min) at different temperatures (37 and 65°C) were performed prior to the staining.

**2.5. Surface immunoprecipitation.** Vero cells in a 6-well plate were transfected with 3 µg of F-wt (and derivate mutants)-expressing plasmid DNA per well. 24 hours post transfection the medium was changed to OptiMEM containing 1:2000 anti-FLAG mAb (Sigma Aldrich; SAB4200071) and incubated at 4°C for 1h. Cells were washed with PBS and then incubated with lysis buffer (10 mM Tris-HCl, pH7.4, 150 mM NaCl, 1% deoxycholate, 1% Triton X-100, 0.1% sodium dodecyl sulfate (SDS)) containing protease inhibitor (Roche, complete mix)) at 4°C. Cell lysates were transferred into tubes and centrifuged at 4°C with 16000g for 30min. Supernatants were transferred into new tubes and 15 µl of Dynabeads™ Protein G for Immunoprecipitation (Invitrogen) were added. The tubes were incubated 4 hours at 4°C on a rotating wheel before the beads were washed with PBS containing 0.05% Tween 40 (Merck). The beads were then boiled at 95°C in Laemmli buffer without reducing agent and proteins subjected to Western blot analyses.

**2.6. Western blotting.** Western blots were performed as previously described (Plattet et al., 2009; Wiener et al., 2007). Samples were fractionated on NuPAGE™ 3-8% Tris-Acetate Mini gels (ThermoFisher Scientific) under nonreducing conditions. Separated proteins were transferred to nitrocellulose membranes by electroblotting. The membranes were then incubated with the polyclonal anti-CDV-F antibody (1:1000) (Cherpillod et al., 1999). Following incubation with a peroxidase-conjugated secondary antibody, the membranes were subjected to 1-Step™ TMB (3,3',5,5'-tetramethylbenzidine)-blotting substrate solution (ThermoFisher Scientific), according to the manufacturer's instructions.

**2.7. Protein production, purification and negative-stain electron microscopy**. The previously described solF-GCNt-expressing DNA plasmid was used as template to produce solF-GCNt-V571C (Ader et al., 2013). Both plasmids were sent to a protein production core facility (PECTF, Dr. D. Hacker, EPFL, Switzerland). From 1L of supernatants harvested after 7 days of protein expression in HEK-293T cells grown in suspension, we usually reached yields of about 0.3-0.5 mg for both soluble F proteins (solF-GCNt and solF-GCNt-V571C).

Since both recombinant proteins harbored a C-terminal HA-tag, affinity purifications were performed using a commercially available agarose beads anti-HA mAb (Covance) and HA peptides for elution. For all four samples, *i.e.*, solF-GCNt and solF-GCNt-V571C in the presence and absence of the inhibitor 3G, 4 µl (~30 µg/ml) were adsorbed for 5 s to parlodion carbon-coated copper grids rendered hydrophilic by glow discharge at low pressure in air. Grids were washed with three drops of double-distilled water and stained with 2 drops of 0.75% uranyl formate. Images were recorded with a FEI Tecnai Spirit BioTwin transmission electron microscope operated at 80 kV and equipped with a FEI Eagle CCD camera at a magnification of 68'000x.

## 3. Results

**3.1. CDV F cysteine mutants assemble into covalently-linked dimers exhibiting prefusion-like conformations.** We previously reported that introducing a cysteine residue at the most membrane-proximal hydrophobic positions of the measles virus F-stalk domain led to the assembly of covalently-linked dimers with moderate functional impact (presumably through the generation of "dimer-of-trimers") (Brindley et al., 2014). To determine whether engineered disulfide bridges within the CDV F-stalk domain would similarly translate into functional structures and whether such complexes would additionally gain resistance to the fusion inhibitor 3G (an AS-48 chemical analog), we inserted single cysteine amino acid at every predicted core position of the F-stalk region (**Fig. 1A**). It is worth to note that all protein variants also harbored a FLAG-tag in the ectodomain at a previously reported location demonstrated to have only minor impacts on F-refolding and membrane fusion-triggering (Ader et al., 2013). The generated panel of F variants was submitted to a series of established bioassays to determine surface expression, conformational state, membrane fusion activity and oligomerization propensity.

The expression and conformational states of standard and mutant F proteins at the cell surface of transfected Vero cells were probed by immunofluorescence and flow cytometric analysis using three previously identified monoclonal antibodies (mAb): an anti-FLAG mAb (recognizing F protein in a conformation-independent manner), an anti-Pre mAb (recognizing the prefusion state) and an anti-Trig mAb (recognizing the postfusion state) (Ader et al., 2013). With the exception of the F-L582C variant, which displayed some intracellular transport-deficiency, all other F-mutants were efficiently expressed at the cell surface (**Fig. 1B**). Most importantly, introducing a single cysteine at every hydrophobic core positions of the putative three-helical bundle of the CDV F-stalk domain did not alter the conformational state of the trimer: all F proteins readily folded into prefusion-like states (**Fig. 1B**).

To determine whether the CDV F cysteine variants formed the expected disulfide bridges (generating covalently-linked F-dimers), the different proteins were expressed in Vero cells and cell surface antigenic material was immunoprecipitated using an anti-FLAG mAb. Proteins were then submitted to Western blot analyses performed under non-reducing conditions. Consistent with our previous data obtained with similar MeV F variants (Brindley et al., 2014), all mutated CDV F proteins exhibited obvious covalently-linked dimeric populations. In sharp contrast, wild-type F proteins exclusively displayed the expected monomeric (F0) population (**Fig. 2**). The profile of migration of CDV F mutants harboring the combination of L596C and V599C ("double") or I589C, L596C and V599C ("triple") cysteine substitutions were also investigated. Interestingly, while the "double" F mutant mostly migrated in the gels as dimeric and trimeric populations, the "triple" F variant exhibited even

higher oligomers (**Fig. 2**). As control, we also mutated residues I564 and G572 of CDV F into cysteines (referred to as the "twin" mutant). It was reported that substituting the two homologous positions of MeV F proteins resulted in inter-monomeric disulfide bonds formation at the interface of the stalk and head domain, thereby generating covalent prefusion F-trimers characterized biochemically and by dithiothreitol (DTT)-dependent reversible fusion activity profiles (Lee et al., 2007). When the CDV F-I564C/G572C "twin" cysteine mutant was subjected to Western blot analysis performed under similar conditions, a covalently-linked trimeric population was indeed readily stabilized (**Fig. 2**).

Collectively, these data demonstrated that the F proteins carrying cysteines at every core position of the stalk domain readily formed covalently-linked dimers, which were properly transported to the cell surface in prefusion-like conformations.

**3.2. "Top-stalk" CDV F cysteine mutants exhibit resistance to 3G.** We next investigated whether the F cysteine mutants preserved proper bioactivity and whether those mutants would additionally remain sensitive towards the small-molecule fusion inhibitor compound 3G. Membrane fusion activity of the diverse F cysteine variants was thus investigated both qualitatively and quantitatively in presence and absence of the inhibitor, using an adapted protocol recently described (Herren et al., 2018).

In absence of 3G and compared to F-wt, "top-stalk" F-L575C, A578C and S582C mutants exhibited only slight impairments in membrane fusion triggering (**Fig. 3A and B**), whereas F-L571C featured about 40% activity. Conversely, "bottom-stalk" F variants harboring cysteine substitutions at position 585, 589 and 592 displayed severe functional defects (**Fig. 3A and B**). However, the two most membrane-proximal F cysteine mutants (F-L596C and F-V599C) exhibited substantial bioactivity. Noteworthy, the "double" and "triple" F mutants were strongly impaired in promoting membrane fusion (**Fig. 3A and B**). Remarkably, in presence of high concentration of 3G (75 μM), CDV F-V571C and F-L575C displayed resistance to the fusion inhibitor, whereas all other mutants remained strongly sensitive, consistent with the profile of inhibition observed in case of F-wt (**Fig. 3A and B**).

To demonstrate that the engineered disulfide bridges contributed to the functional defects of some "bottom-stalk" F cysteine mutants, F-expressing cells were treated 30 min with a mild concentration of DTT (50 mM) to potentially reduce the covalent bonds and eventually restore membrane fusion induction. In this series of experiments, we selected the F cysteine variants S592C and "triple", because exhibiting severe functional impairments. As positive control, we employed the above described "twin" F cysteine variant. In addition, upon DTT treatment, cells were treated (or not) with 3G to determine the sensitivity of the selected F variants to the fusion inhibitor. Strikingly, while both "bottom-stalk" F cysteine mutants exhibited some restoration of membrane fusion activity upon DTT treatment, they remained

entirely sensitive to the fusion inhibitor compound (**Fig. 4**). In sharp contrast, the "twin" mutant (I564C/G572C), which was indeed reactivated upon DTT treatment, displayed some resistance to 3G, since fusion activity could be recorded (**Fig. 4**).

Overall, these data demonstrated that CDV F proteins carrying cysteine substitutions at positions 571, 575, 564 and 572 (the two latter in combination), all locating at the top of the stalk region, displayed resistance to 3G. Conversely, "bottom-stalk" F cysteine mutants remained fully sensitive to the fusion inhibitor.

**3.3. "Top-stalk" CDV F cysteine mutants escaped 3G-mediated stabilization upon heat shock.** The prefusion MeV F crystal structure in complex with AS-48 highlighted the interacting residues (Hashiguchi et al., 2018). Previously identified critical residues of resistance mutations against AS-48 (*e.g.* F-N462K) (Doyle et al., 2006) indeed locate in the binding pocket (Hashiguchi et al., 2018). A structurally-diverse MeV F inhibitor (fusion inhibitor peptide [FIP]; (Richardson et al., 1980)) was suggested (Ha et al., 2017), and now proven (Hashiguchi et al., 2018), to dock at the identical microdomain. Most FIP-resistance mutations (which also conferred resistance to AS-48) were indeed part of the hydrophobic pocket binding site (*e.g*. I452, D458, V459, N462 and G464) (Ha et al., 2017). Interestingly, CDV F residues V571, L575, I564 and G572 putatively locate in close proximity to the homologous residues of those MeV F amino acids, which therefore suggest a primary resistance mechanism.

We previously developed an assay, which enabled us to identify the stabilizing impact of 3G on prefusion F trimers. The assay relied on binding of F conformation-specific mAbs after heat shock treatment, to artificially trigger refolding. This strategy enabled us to accurately assess the "temperature of refolding", thus indirectly informing about F trimers' intrinsic stability. Strikingly, if 3G docked onto prefusion F complexes, the temperature of refolding was increased by around 5-10°C (Avila et al., 2014). To indirectly determine whether 3G was still able to bind and stabilize the prefusion conformation of the designed F cysteine mutants, we adapted this assay by employing two mAbs: anti-Pre (recognizing the prefusion state) and anti-FLAG (recognizing the FLAG-tag and indicating cell surface expression). The impact of 3G on prefusion F states was thus determined by calculating the ratio between the binding capacities of the anti-Pre and anti-FLAG mAbs (determined by flow cytometry). Such experiments were conducted either at physiological temperature (37°C) or after a brief heat shock (5min, 65°C) in presence or absence of the fusion inhibitor.

At 37°C, selected "top-stalk" (V571C and L578C) and "bottom-stalk" (L596C and V599C) F protein variants exhibited very similar proportion of prefusion states trimers in the presence or absence of 3G (**Fig. 5A**). When data were normalized to conditions performed in the absence of 3G, similar profiles were highlighted (**Fig. 5B**). Interestingly however, in 3G-

treated cells and upon brief heat shock at 65°C, a considerable amount of prefusion F trimers could still be detected in case of F-wt and the two “bottom-stalk” F cysteine variants (L596C and F-V599C) as compared to “top-stalk” mutants (**Fig. 5C**). The differences became even more apparent when data were normalized to conditions performed in the absence of the drug (**Fig. 5D**). Interestingly, the “twin” mutant displayed an intermediate phenotype; although 3G could still impact the prefusion state to some extent (**Fig. 5C**), the stabilizing effect was clearly less potent as compared to the one exerted on mutants F-L596C and F-V599C (**Fig. 5D**). Note also that prefusion states of tested “bottom and top-stalk” F cysteines mutants were slightly destabilized as compared to F-wt, since, in absence of 3G, F-wt seemed to be less temperature-sensitive as seen after a brief heat shock (**Fig. 5C**). Conversely, in absence of the drug, the “twin” mutant featured wt-like stability (**Fig. 5C**).

Taken together, our data demonstrated that the drug-resistant “top-stalk” CDV F cysteine mutant did not exhibit 3G-mediated stabilization of prefusion states (F-V571C and F-L575C), or only to limited extent (“twin” F-I564C/G572C variant). This suggested that resistance resulted from lack of efficient docking of the compound on those mutated prefusion F-structures. Since CDV F amino acids I564, V571, G572 and L575 are all potentially part of the hydrophobic pocket, these findings revealed that prefusion CDV and MeV F trimers are likely sharing substantial structural similarities. It is therefore expected that 3G presumably docks onto the same pocket as AS-48 did on prefusion MeV F structures (Hashiguchi et al., 2018).

**3.4. Unmodified soluble F proteins preferentially display a “prefusion-like” state in presence of 3G.** To provide more direct evidence that 3G may indeed exert a stabilization effect on prefusion CDV F trimers, we expressed a previously reported soluble F construct (solF) in HEK-293T cells (Ader et al., 2013). The latter was engineered to carry a trimeric GCN4 motif (GCNt) in place of the transmembrane and cytoplasmic tail domains (solF-GCNt). In parallel, we inserted the V571C mutation into the soluble protein (solF-GCNt-V571C) and expressed it under similar conditions. After affinity purification, both recombinant soluble proteins were submitted to SDS-PAGE migration performed under non-reducing conditions and were subsequently revealed by Coomassie staining. As expected from our previous analysis, while solF-GCNt exclusively migrated as a monomeric population, solF-GCNt-V571C displayed both monomers and dimers, which corroborated the results obtained with their full-length membrane-anchored counterparts (**Fig. 6A**).

Next, both recombinant soluble proteins were expressed in the presence or absence of 3G (75 µM) and purified proteins were analyzed by negative-stain electron microscopy. Interestingly, in the absence of the compound, both soluble proteins exhibited a mixed population of either “tree”-like globular structures (presumably prefusion states) or “golf-tee”-

like elongated conformations (presumably postfusion states) (**Fig. 6B and C**). This indicated that, despite soluble F proteins harboring the prefusion-stabilizing trimerization motif, spontaneous refolding into postfusion states did occur in a considerable number of F-trimers. Remarkably, in the presence of 3G, a substantial number of solF-GCNt displayed the prefusion state, whereas solF-GCNt-V571C exhibited unaltered mixed conformational populations (**Fig. 6Band C**). These findings not only validated that 3G had no impact on prefusion states of “top-stalk” F cysteine mutants, but also that metastable conformations of standard F trimers were readily stabilized by the fusion inhibitor.

## 4. Discussion

Molecular understanding of the mode-of-action and associated potential resistance mechanisms of a given antiviral is supportive to its usage in clinic. It was reported that the small-molecule fusion blocker AS-48 class compounds may exert their inhibitory function by stabilizing prefusion morbilliviral F structures (Avila et al., 2014; Doyle et al., 2006). The recently determined prefusion MeV F structure in complex with AS-48 demonstrated that the fusion inhibitor bound to three hydrophobic pocket microdomains located at the interface of the head and stalk domains (**Fig. 7A**; CDV F model) (Hashiguchi et al., 2018). Since mutations within and around this region led to hyperfusogenic F profiles, a functional role of the head-stalk interface in the F-triggering/refolding process was suggested (Doyle et al., 2006; Jurgens et al., 2015; Lee et al., 2007; Watanabe et al., 2015; Watanabe et al., 2013). Additionally, since some of those AS-48 resistant mutants exhibited intracellular transport-deficiency in the absence of the compound, which was restored in its presence, a stabilizing role of the inhibitor on prefusion MeV F complexes was inferred (Doyle et al., 2006). Here, we conducted comprehensive mechanistic and low-resolution structural analyses to determine whether engineered disulfide bridges within the CDV F-stalk domain may provide resistance profiles to 3G, an AS-48 chemical analog compound.

We recently demonstrated that cysteine substitutions performed in the MeV F-stalk translated into membrane fusion triggering-competent, covalently-linked, F dimers. Such productive F complexes were hypothesized to result from the assembly of putative dimer-of-trimers (Brindley et al., 2014). Considering that the base of the globular head is quite large as compared to the compact helical bundle stalk region, structural flexibility within at least one monomer of two neighboring F trimers must be considerable in order to allow, stalk-dependent, inter-trimers disulfide bond formation. We thus employed this approach to rationally engineer conformational distortions within the CDV F-stalk region and potentially disturb the binding efficacy of the drug.

Consistent with data obtained in the context of MeV F (Brindley et al., 2014), introducing cysteine residues at every hydrophobic core positions within the three-helix bundle stalk domain of prefusion CDV F led to the generation of covalently-linked dimeric complexes. Such complexes may fold into covalently-linked dimer-of-trimers, which would indeed require a certain degree of structural freedom within the F-stalk region to achieve productive prefusion architectures. Based on the findings collected in this study, we further hypothesize that structural flexibility within the morbilliviral F-stalk domain may potentially occur only locally. Local structural flexibility within the stalk may preserve the membrane-distal 3G binding sites unaltered when disulfide bonds are engineered membrane-proximal. Conversely, introducing supplementary covalent bonds at the top of the stalk may directly (or indirectly) affect the 3G binding sites (**Fig. 8A and B**).

Three lines of evidence support our model. Firstly, mutations conferring resistance to the morbillivirus fusion inhibitor Z-D-Phe-L-Phe-Gly peptide (FIP) were recently mapped to the structural transition between the globular head and the stalk domain (Ha et al., 2017). Because most of the FIP-resistance mutations were demonstrated to also provide resistance to AS-48, both fusion inhibitors were suggested to bind to the same microdomain on prefusion MeV F structures (Ha et al., 2017). Interestingly, in MeV F/inhibitor co-crystal structures, most of the resistance mutations were located at the rim and/or at the bottom of the deep hydrophobic pocket shown to accommodate the benzene group of AS-48 and FIP (**Fig. 7B and C**) (Hashiguchi et al., 2018). Taken together, since the MeV F homologous amino acids to CDV F residues I564, V571, G572 and L575 ("top-stalk" mutants), all map within the AS-48 binding site, it is not unexpected that 3G would bind to same microdomains on prefusion CDV F structures.

Secondly, our data provided clear evidence that "top-stalk" CDV F cysteine variants (F-V571C and F-L575C) gained resistance to 3G, whereas "bottom-stalk" variants remained sensitive to the drug. In addition, drug-resistance phenotypes were also recorded with the "twin" F cysteine mutant, which harbors two mutations locating at the top of the stalk and at the base of the head domain. These data highlighted the intriguing notion that resistance or sensitivity to 3G relied on the position of the covalent bond engineered within the CDV F-stalk region. However, whether the 3G-resistance profiles of "top-stalk" mutants resulted from lack of hydrophobicity within the binding site, direct disruption of the pocket, or an overall F structure incompatible to 3G binding (long-range effect) warrants further investigations.

Thirdly, we demonstrated that the prefusion conformations of "bottom-stalk" F cysteine mutants gained resistance to heat shock treatments in presence of the drug. Conversely, prefusion states of "top-stalk" CDV F cysteine variants remained sensitive to heat treatments regardless of the presence or absence of the fusion inhibitor. It is worth to note that 3G could still stabilize the "twin" F mutants to some extent. However, the impact was substantially less potent than the effect exerted on other "bottom-stalk" F mutants, which suggested a partial drug-resistance profile of the "twin" mutant. These data therefore argued for the inability of the drug to efficiently bind to those "top-stalk" CDV F mutated trimers and consequently highlighted a potential primary site resistance mechanism (direct or indirect). Interestingly, in a previous study, we identified F mutants harboring substitutions locating within a microdomain at the center of the F globular head domain, and those mutated F proteins similarly displayed resistance to 3G. However, in contrast the "top-stalk" cysteine F mutants designed in this study, the "central pocket" F mutants remained still strongly stabilized by the compound, which rather provided evidence for a secondary resistance mechanism (Avila et al., 2014).

Low-resolution electron microscopy experiments were additionally strongly suggestive for a stabilizing impact of 3G on prefusion F trimers and for a primary site resistance mechanism exhibited by “top-stalk” F cysteine mutants. Indeed, solF-GCNt exhibited a mixed population with roughly 50% of F proteins preserving the prefusion state, whereas the other 50% spontaneously refolded into the postfusion state. Although this clearly illustrated that GCNt trimerization motifs were not sufficient to completely maintain these F trimers in the prefusion conformation, it however underlined the stabilizing impact of 3G. In presence of the fusion inhibitor, mixed F structures switched to a much more homogenous F population, characterized by the almost exclusive presence of prefusion state solF-GCNt. Even though prefusion MeV F-trimers are likely equally stabilized by AS-48, the phenotype could not be monitored in high-resolution structural analyses, since the apo-state was already stabilized through the engineering of disulfide bonds within the bottom of the stalk domain (Hashiguchi et al., 2018). Finally, our structural analyses unambiguously indicated that 3G lost its prefusion-stabilizing impact when tested on a soluble “top-stalk” F cysteine variant (solF-GCNt-V571C). Overall these data provided further evidence for the mode-of-action of 3G-mediated fusion inhibition and associated mechanisms of resistance.

To date, high-resolution structures of pneumovirus and paramyxovirus prefusion F trimers in complex with structurally diverse fusion inhibitory compounds are available for respiratory syncytial virus (RSV) and measles virus (Battles et al., 2016; Hashiguchi et al., 2018). Remarkably, in RSV F crystal structures, all chemical compounds bound to a threefold-axis internal central pocket locating at the base of the globular head domain. Thus, different binding sites were determined between fusion inhibitors acting on RSV or MeV F proteins. Considering the high mutational rates of polymerase of envelope RNA viruses and the demonstrated high propensity of emergence of drug-resistant viral variants, as well as structural similarities between RSV and MeV F trimers, it may be attractive to rationally develop second generation of RSV F inhibitors potentially binding to pocket microdomains mimicking those targeted by AS-48 and FIP in MeV F.

## Funding

This work was supported by the University of Bern, the Swiss National Science Foundation (Refs. No. 310030_173185 to P.P. and No. 31003A_162581 to D.F.), and the National Centres of Competence in Research (NCCRs) TransCure and Molecular Systems Engineering to D.F.

## Conflict of interest

The authors declare that they have no conflict of interest.

## Ethical approval

This article does not contain any studies with human participants or animals performed by any of the authors.


## Acknowledgments

We thank Yusuke Yanagi for providing us with receptor expressing Vero cells. We are also very thankful for receiving plasmids from Zene Matsuda.


## References


Ader-Ebert, N., Khosravi, M., Herren, M., Avila, M., Alves, L., Bringolf, F., Orvell, C., Langedijk, J.P., Zurbriggen, A., Plemper, R.K., Plattet, P., 2015. Sequential conformational changes in the morbillivirus attachment protein initiate the membrane fusion process. PLoS Pathog. 11(5), e1004880.

Ader, N., Brindley, M., Avila, M., Orvell, C., Horvat, B., Hiltensperger, G., Schneider-Schaulies, J., Vandevelde, M., Zurbriggen, A., Plemper, R.K., Plattet, P., 2013. Mechanism for active membrane fusion triggering by morbillivirus attachment protein. J.Virol. 87(1), 314-326.

Ader, N., Brindley, M.A., Avila, M., Origgi, F.C., Langedijk, J.P., Orvell, C., Vandevelde, M., Zurbriggen, A., Plemper, R.K., Plattet, P., 2012. Structural rearrangements of the central region of the morbillivirus attachment protein stalk domain trigger F protein refolding for membrane fusion. J.Biol.Chem. 287(20), 16324-16334.

Apte-Sengupta, S., Navaratnarajah, C.K., Cattaneo, R., 2013. Hydrophobic and charged residues in the central segment of the measles virus hemagglutinin stalk mediate transmission of the fusion-triggering signal. J.Virol. 87(18), 10401-10404.

Avila, M., Alves, L., Khosravi, M., Ader-Ebert, N., Origgi, F., Schneider-Schaulies, J., Zurbriggen, A., Plemper, R.K., Plattet, P., 2014. Molecular determinants defining the triggering range of prefusion F complexes of canine distemper virus. Journal of virology 88(5), 2951-2966.

Battles, M.B., Langedijk, J.P., Furmanova-Hollenstein, P., Chaiwatpongsakorn, S., Costello, H.M., Kwanten, L., Vranckx, L., Vink, P., Jaensch, S., Jonckers, T.H., Koul, A., Arnoult, E., Peeples, M.E., Roymans, D., McLellan, J.S., 2016. Molecular mechanism of respiratory syncytial virus fusion inhibitors. Nat.Chem.Biol. 12(2), 87-93.

Brindley, M.A., Plattet, P., Plemper, R.K., 2014. Efficient replication of a paramyxovirus independent of full zippering of the fusion protein six-helix bundle domain. Proc.Natl.Acad.Sci.U.S.A 111(36), E3795-3804.

Brindley, M.A., Takeda, M., Plattet, P., Plemper, R.K., 2012. Triggering the measles virus membrane fusion machinery. Proc.Natl.Acad.Sci.U.S.A 109(44), E3018-E3027.

Cherpillod, P., Beck, K., Zurbriggen, A., Wittek, R., 1999. Sequence analysis and expression of the attachment and fusion proteins of canine distemper virus wild-type strain A75/17. J.Virol. 73(3), 2263-2269.

Doyle, J., Prussia, A., White, L.K., Sun, A., Liotta, D.C., Snyder, J.P., Compans, R.W., Plemper, R.K., 2006. Two domains that control prefusion stability and

transport competence of the measles virus fusion protein. J.Virol. 80(3), 1524-1536.

Feng, N., Yu, Y., Wang, T., Wilker, P., Wang, J., Li, Y., Sun, Z., Gao, Y., Xia, X., 2016. Fatal canine distemper virus infection of giant pandas in China. Scientific reports 6, 27518.

Ha, M.N., Delpeut, S., Noyce, R.S., Sisson, G., Black, K.M., Lin, L.T., Bilimoria, D., Plemper, R.K., Prive, G.G., Richardson, C.D., 2017. Mutations in the Fusion Protein of Measles Virus That Confer Resistance to the Membrane Fusion Inhibitors Carbobenzoxy-d-Phe-l-Phe-Gly and 4-Nitro-2-Phenylacetyl Amino-Benzamide. Journal of virology 91(23).

Hashiguchi, T., Fukuda, Y., Matsuoka, R., Kuroda, D., Kubota, M., Shirogane, Y., Watanabe, S., Tsumoto, K., Kohda, D., Plemper, R.K., Yanagi, Y., 2018. Structures of the prefusion form of measles virus fusion protein in complex with inhibitors. Proceedings of the National Academy of Sciences of the United States of America.

Herren, M., Shrestha, N., Wyss, M., Zurbriggen, A., Plattet, P., 2018. Regulatory Role of the Morbillivirus Attachment Protein Head-to-Stalk Linker Module in Membrane Fusion Triggering. Journal of virology 92(18).

Jin, Y., Zhang, X., Ma, Y., Qiao, Y., Liu, X., Zhao, K., Zhang, C., Lin, D., Fu, X., Xu, X., Wang, Y., Wang, H., 2017. Canine distemper viral infection threatens the giant panda population in China. Oncotarget 8(69), 113910-113919.

Jurgens, E.M., Mathieu, C., Palermo, L.M., Hardie, D., Horvat, B., Moscona, A., Porotto, M., 2015. Measles fusion machinery is dysregulated in neuropathogenic variants. mBio 6(1).

Krumm, S.A., Yan, D., Hovingh, E.S., Evers, T.J., Enkirch, T., Reddy, G.P., Sun, A., Saindane, M.T., Arrendale, R.F., Painter, G., Liotta, D.C., Natchus, M.G., von, M., V, Plemper, R.K., 2014. An orally available, small-molecule polymerase inhibitor shows efficacy against a lethal morbillivirus infection in a large animal model. Sci.Transl.Med. 6(232), 232ra252.

Lamb, R.A., Parks, G.D., 2007. Paramyxoviridae: The viruses and their replication. In: Fileds, B., Knipe, D.M., Howley, P.M. (Eds.), Paramyxoviridae: The viruses and their replication. Fields' Virology, Fifth edition. Lippincott Williams & Wilkins, Philadelphia, pp. 1449-1496.

Lee, J.K., Prussia, A., Snyder, J.P., Plemper, R.K., 2007. Reversible inhibition of the fusion activity of measles virus F protein by an engineered intersubunit disulfide bridge. J.Virol. 81(16), 8821-8826.

Mathieu, C., Huey, D., Jurgens, E., Welsch, J.C., DeVito, I., Talekar, A., Horvat, B., Niewiesk, S., Moscona, A., Porotto, M., 2015. Prevention of Measles Virus Infection by Intranasal Delivery of Fusion Inhibitor Peptides. Journal of virology 89(2), 1143-1155.

McLellan, J.S., Chen, M., Leung, S., Graepel, K.W., Du, X., Yang, Y., Zhou, T., Baxa, U., Yasuda, E., Beaumont, T., Kumar, A., Modjarrad, K., Zheng, Z., Zhao, M., Xia, N., Kwong, P.D., Graham, B.S., 2013. Structure of RSV fusion glycoprotein trimer bound to a prefusion-specific neutralizing antibody. Science 340(6136), 1113-1117.

Navaratnarajah, C.K., Kumar, S., Generous, A., pte-Sengupta, S., Mateo, M., Cattaneo, R., 2014. The measles virus hemagglutinin stalk: structures and functions of the central fusion activation and membrane-proximal segments. J.Virol. 88(11), 6158-6167.

Navaratnarajah, C.K., Negi, S., Braun, W., Cattaneo, R., 2012. Membrane fusion triggering: three modules with different structure and function in the upper half

of the measles virus attachment protein stalk. J.Biol.Chem. 287(46), 38543-38551.

Plattet, P., Alves, L., Herren, M., Aguilar, H.C., 2016. Measles Virus Fusion Protein: Structure, Function and Inhibition. Viruses 8(4), 112.

Plattet, P., Cherpillod, P., Wiener, D., Zipperle, L., Vandevelde, M., Wittek, R., Zurbriggen, A., 2007. Signal peptide and helical bundle domains of virulent canine distemper virus fusion protein restrict fusogenicity. J.Virol. 81(20), 11413-11425.

Plattet, P., Langedijk, J.P., Zipperle, L., Vandevelde, M., Orvell, C., Zurbriggen, A., 2009. Conserved leucine residue in the head region of morbillivirus fusion protein regulates the large conformational change during fusion activity. Biochemistry 48(38), 9112-9121.

Plattet, P., Rivals, J.P., Zuber, B., Brunner, J.M., Zurbriggen, A., Wittek, R., 2005. The fusion protein of wild-type canine distemper virus is a major determinant of persistent infection. Virology 337(2), 312-326.

Plemper, R.K., Erlandson, K.J., Lakdawala, A.S., Sun, A., Prussia, A., Boonsombat, J., ki-Sener, E., Yalcin, I., Yildiz, I., Temiz-Arpaci, O., Tekiner, B., Liotta, D.C., Snyder, J.P., Compans, R.W., 2004. A target site for template-based design of measles virus entry inhibitors. Proc.Natl.Acad.Sci.U.S.A 101(15), 5628-5633.

Richardson, C.D., Scheid, A., Choppin, P.W., 1980. Specific inhibition of paramyxovirus and myxovirus replication by oligopeptides with amino acid sequences similar to those at the N-termini of the F1 or HA2 viral polypeptides. Virology 105(1), 205-222.

Russell, C.J., Jardetzky, T.S., Lamb, R.A., 2001. Membrane fusion machines of paramyxoviruses: capture of intermediates of fusion. EMBO J. 20(15), 4024-4034.

Sakai, K., Nagata, N., Ami, Y., Seki, F., Suzaki, Y., Iwata-Yoshikawa, N., Suzuki, T., Fukushi, S., Mizutani, T., Yoshikawa, T., Otsuki, N., Kurane, I., Komase, K., Yamaguchi, R., Hasegawa, H., Saijo, M., Takeda, M., Morikawa, S., 2013. Lethal canine distemper virus outbreak in cynomolgus monkeys in Japan in 2008. J.Virol. 87(2), 1105-1114.

Simons, E., Ferrari, M., Fricks, J., Wannemuehler, K., Anand, A., Burton, A., Strebel, P., 2012. Assessment of the 2010 global measles mortality reduction goal: results from a model of surveillance data. Lancet 379(9832), 2173-2178.

Singethan, K., Hiltensperger, G., Kendl, S., Wohlfahrt, J., Plattet, P., Holzgrabe, U., Schneider-Schaulies, J., 2010. N-(3-Cyanophenyl)-2-phenylacetamide, an effective inhibitor of morbillivirus-induced membrane fusion with low cytotoxicity. J.Gen.Virol. 91(Pt 11), 2762-2772.

Sun, A., Prussia, A., Zhan, W., Murray, E.E., Doyle, J., Cheng, L.T., Yoon, J.J., Radchenko, E.V., Palyulin, V.A., Compans, R.W., Liotta, D.C., Plemper, R.K., Snyder, J.P., 2006. Nonpeptide inhibitors of measles virus entry. J.Med.Chem. 49(17), 5080-5092.

Watanabe, S., Ohno, S., Shirogane, Y., Suzuki, S.O., Koga, R., Yanagi, Y., 2015. Measles virus mutants possessing the fusion protein with enhanced fusion activity spread effectively in neuronal cells, but not in other cells, without causing strong cytopathology. Journal of virology 89(5), 2710-2717.

Watanabe, S., Shirogane, Y., Suzuki, S.O., Ikegame, S., Koga, R., Yanagi, Y., 2013. Mutant fusion proteins with enhanced fusion activity promote measles virus spread in human neuronal cells and brains of suckling hamsters. J.Virol. 87(5), 2648-2659.

Wiener, D., Plattet, P., Cherpillod, P., Zipperle, L., Doherr, M.G., Vandevelde, M., Zurbriggen, A., 2007. Synergistic inhibition in cell-cell fusion mediated by the matrix and nucleocapsid protein of canine distemper virus. Virus Res. 129(2), 145-154.

Wong, J.J., Paterson, R.G., Lamb, R.A., Jardetzky, T.S., 2016. Structure and stabilization of the Hendra virus F glycoprotein in its prefusion form. Proc.Natl.Acad.Sci.U.S.A 113(4), 1056-1061.

Xu, K., Chan, Y.P., Bradel-Tretheway, B., Akyol-Ataman, Z., Zhu, Y., Dutta, S., Yan, L., Feng, Y., Wang, L.F., Skiniotis, G., Lee, B., Zhou, Z.H., Broder, C.C., Aguilar, H.C., Nikolov, D.B., 2015. Crystal Structure of the Pre-fusion Nipah Virus Fusion Glycoprotein Reveals a Novel Hexamer-of-Trimers Assembly. PLoS Pathog. 11(12), e1005322.

Yin, H.S., Wen, X., Paterson, R.G., Lamb, R.A., Jardetzky, T.S., 2006. Structure of the parainfluenza virus 5 F protein in its metastable, prefusion conformation. Nature 439(7072), 38-44.

## FIGURE LEGENDS

**Figure 1. Characterization of CDV F-mutants harboring cysteine substitution at every hydrophobic core position of the putative helical bundle stalk region.** (A) Side view of prefusion CDV F-trimer, which consists of a globular head and stalk domains. The model was generated from the related PIV5 prefusion F-structure (PDB code: 2B9B). The 3-helix bundle stalk domain and derived 7-mer core hydrophobic positions *("a"* and *"d"*) are highlighted on the right side. The three monomers are color-coded in yellow, cyan and red. pm: plasma membrane. (B) Conformational probing of surface-exposed F proteins was performed using three different mAbs: anti-FLAG (conformation-independent; grey bars), anti-Pre (prefusion-specific; green bars) and anti-Trig (postfusion-specific; red bars). Upon addition of Alexa-fluor-conjugated secondary antibody, F-expressing cells were detached and submitted to flow cytometry analyses to record quantitative data. Means and standard deviations of data from three independent experiments performed in triplicates are shown. Double: CDV F-L596C/V599C; triple: CDV F-I589C/L596C/V599C.

**Figure 2. Biochemical analyses of the panel of CDV F cysteine mutants.** To investigate oligomeric profiles, Vero cells were transfected with the various F-expressing plasmids. 24 hours post-transfections, cell surface F-antigenic materials were immunoprecipitated and submitted to Western blot analyses performed under nonreducing conditions. M: F-monomers; D: F-dimers; T: F-trimers; HO: F-high order oligomers. Double: CDV F-L596C/V599C; triple: CDV F-I589C/L596C/V599C; twin: CDV F-I564C/G572C.

**Figure 3. Top-stalk CDV F cysteine mutants readily escape 3G-mediated fusion inhibition.** (A) F proteins were co-expressed with H-proteins in Vero-cSLAM cells and treated, or not, with 75 µM of 3G. Assessment of cell-cell fusion induction was performed by taking pictures of representative fields of view 24 hours post-transfection. (B) Quantitative assessment of cell-cell fusion induction in presence or absence of 75 µM of 3G. Means ± standard deviations of data from two independent experiments performed in triplicates are shown. Double: CDV F-L596C/V599C; triple: CDV F-I589C/L596C/V599C.

**Figure 4. Impact of the engineered disulfide bonds on non-functional F cysteine mutants.** The cell-cell fusion capacity of the "twin" (I564C/G572C), "triple" (I589C/L596C/V599C) and S592C F cysteine mutants were analyzed by regular cell-cell fusion assay using Vero-cSLAM cells. To assess the potential reversible fusion inhibition

profiles of the various F proteins, Vero-cSLAM cells were treated 30 min, 24 hours post-transfections, with a mild concentration (50 mM) of dithiothreitol (+DTT), or left untreated (-DTT). In the indicated conditions, 3G (75 µM) was added post DTT-treatments.

**Figure 5. Heat shock-resistance profiles of perfusion F conformations in presence or absence of the fusion inhibitor compound.** (A-B) Selected F proteins were expressed in Vero cells for 24 hours. Cells were then subjected to brief heat shocks (5 min) at 37°C (A) or 65°C (B) in the presence or absence of 75 µM of 3G. Conformational probing of surface-exposed F proteins was performed using two different mAbs: anti-FLAG (conformation-independent) and anti-Pre (prefusion-specific). Upon addition of Alexa-fluor-conjugated secondary antibody, F-expressing cells were detached and submitted to flow cytometry analyses to record quantitative data. (C-D) For each F-protein, values obtained in the presence of 3G (+3G) were normalized to values obtained in the absence of the drug (-3G) and set to 1. Means ± standard deviations of data from three independent experiments performed in duplicates are shown.

**Figure 6. Biochemical and negative stain electron microscopy analyses of purified solF-GCNt and solF-GCNt-V571C in the absence and presence of the inhibitor 3G.** (A) Affinity-purified solF proteins were separated by SDS-PAGE migration performed under nonreducing conditions and were revealed by Coomassie staining. M: F-monomers; D: F-dimers. (B) Electron micrographs of negatively-stained solF-GCNt and solF-GCNt-V571C in the absence or presence of the fusion inhibitor 3G (75 µM). Only obvious assignable solF-GCNt and solF-GCNt-V571C proteins in the prefusion and postfusion states are highlighted in yellow and green, respectively. The scale bars represent 100 nm. (C) To collect semi-quantitative data, single F particles in prefusion or postfusion states were counted. Means ± standard deviations of data from several fields of views are shown. An unpaired two-tailed t test was performed to assess significant differences compared to wild-type (*, p-value ≤0.0001)

**Figure 7. Pocket microdomain in CDV F-trimers potentially accommodating the 3G fusion inhibitor compound and associated resistance mutations.** (A) Bottom view of prefusion CDV F-trimer with the three potential 3G-binding sites color-coded in blue (model generated from the MeV F prefusion state in the absence of inhibitory compounds (PDB code: 5YXW)). (B-C) Close-up front view of one pocket microdomain. Residues in contact

with AS-48 in MeV F prefusion state are highlighted in blue (B). Amino acids within the deep hydrophobic pocket microdomain that conferred resistance to morbilliviral inhibitors are shown in red (resistance to AS-48) and cyan (resistance to AS-48 (for MeV F proteins) and 3G (for CDV F proteins)) (C).

**Figure 8. Potential model of covalently-linked F dimer-of-trimers folding and associated mechanism of resistance to a fusion inhibitor (3G)**. F complexes in prefusion conformations are represented. (A) “Top-stalk” and “bottom-stalk” residues V571 and V599, respectively, are shown in red (left side). The putative binding site of 3G is highlighted with three green transparent circles (right side). (B) Model of arrangement of “top-stalk” and “bottom-stalk” covalently-linked dimer-of-trimers. The engineered disulfide bonds are shown in cyan. Residues V571 and V599 are color-coded in red. “Top-stalk” F complexes display disturbed 3G binding site (red transparent circles; left side), whereas “bottom-stalk” F structures feature intact 3G binding sites (green transparent circles). Pm: plasma membrane.

# Figure 1

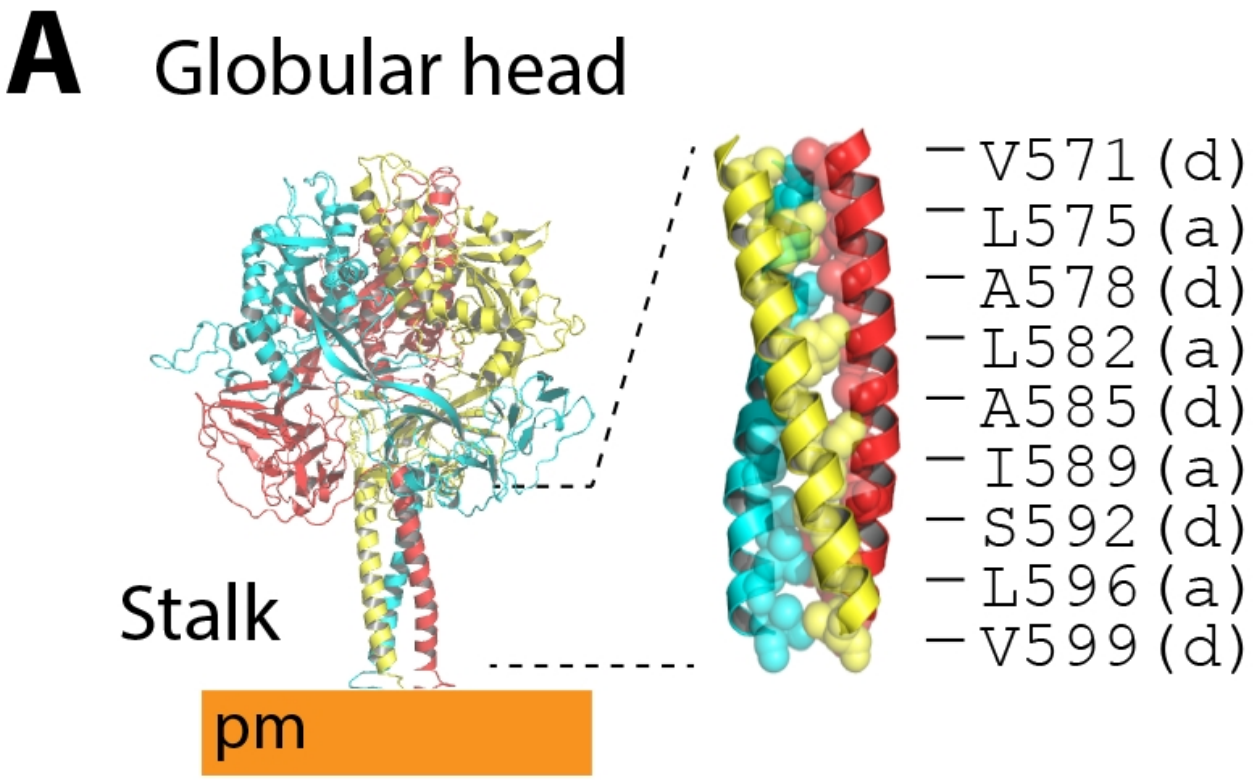
A
Globular head
V571(d)
L575(a)
A578(d)
L582(a)
A585(d)
I589(a)
S592(d)
L596(a)
V599(d)
Stalk
pm

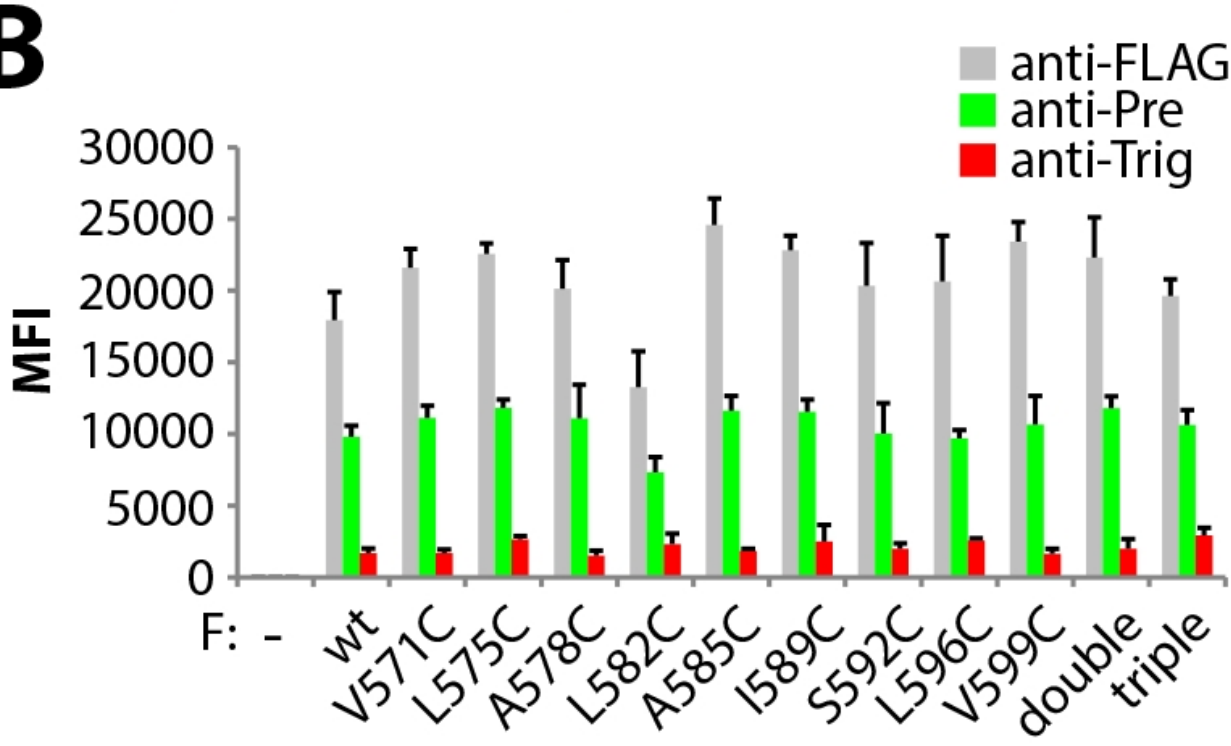
B
anti-FLAG
anti-Pre
anti-Trig
MFI
30000
25000
20000
15000
10000
5000
0
F: -
wt
V571C
L575C
A578C
L582C
A585C
I589C
S592C
L596C
V599C
double
triple

# Figure 2

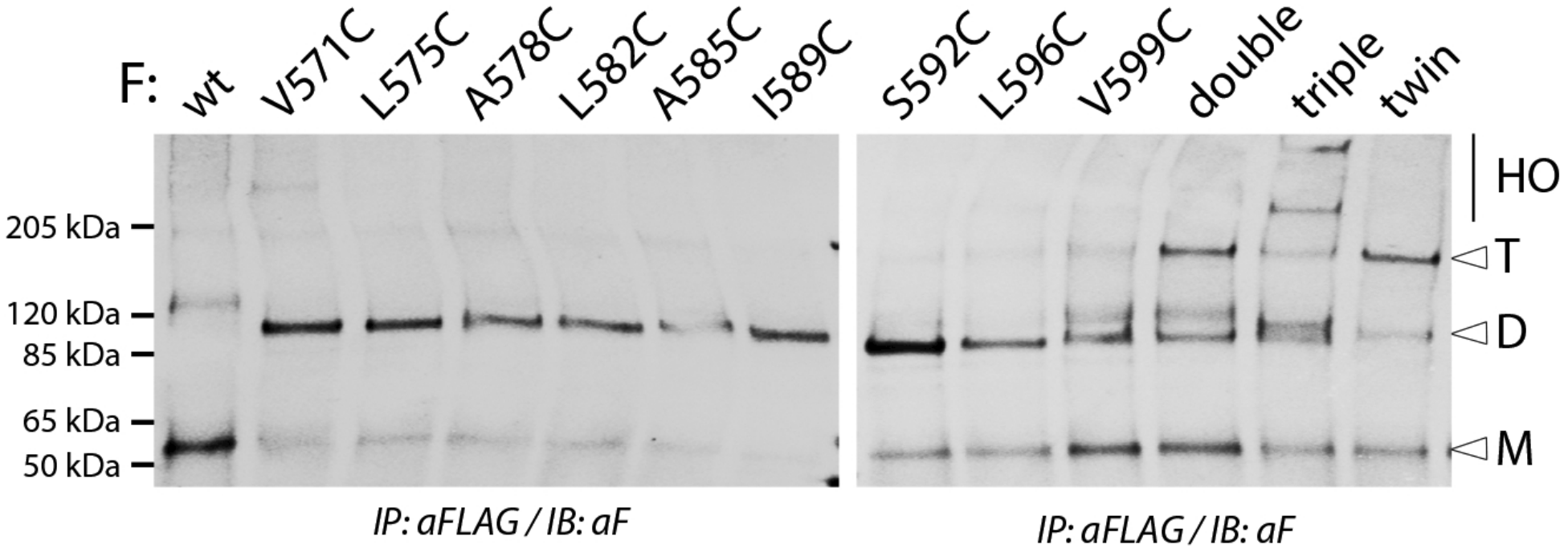
F:
wt
V571C
L575C
A578C
L582C
A585C
I589C
S592C
L596C
V599C
double
triple
twin
205 kDa
120 kDa
85 kDa
65 kDa
50 kDa
HO
T
D
M
IP: aFLAG / IB: aF
IP: aFLAG / IB: aF

Figure 3

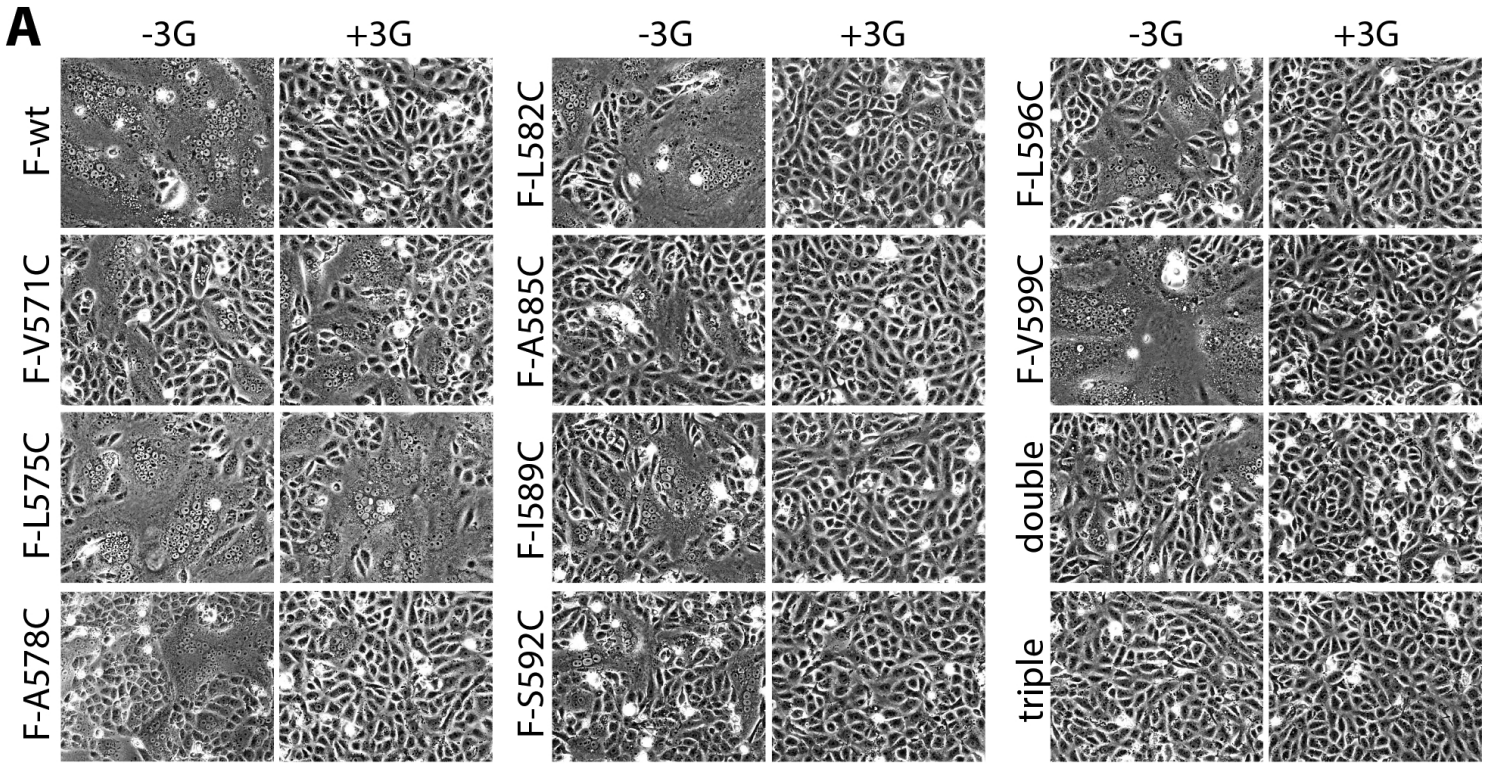
A
-3G
+3G
-3G
+3G
-3G
+3G
F-wt
F-V571C
F-L575C
F-A578C
F-L582C
F-A585C
F-I589C
F-S592C
F-L596C
F-V599C
double
triple

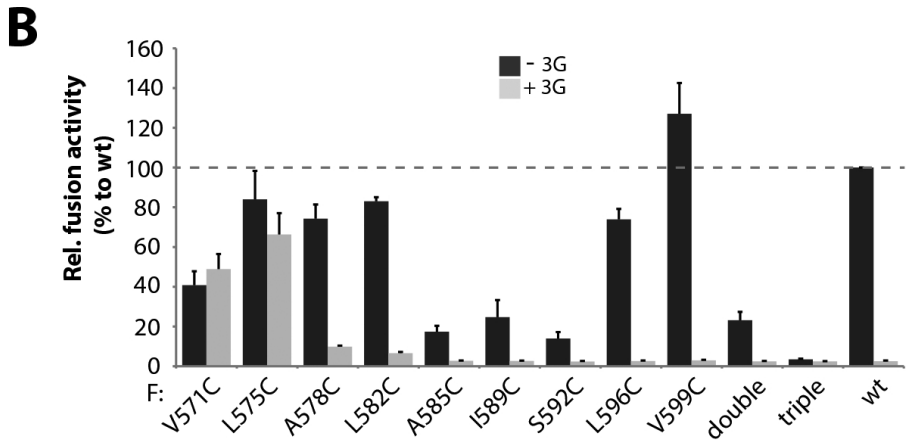
B
Rel. fusion activity (% to wt)
160
140
120
100
80
60
40
20
0
- 3G
+ 3G
F:
V571C
L575C
A578C
L582C
A585C
I589C
S592C
L596C
V599C
double
triple
wt

# Figure 4

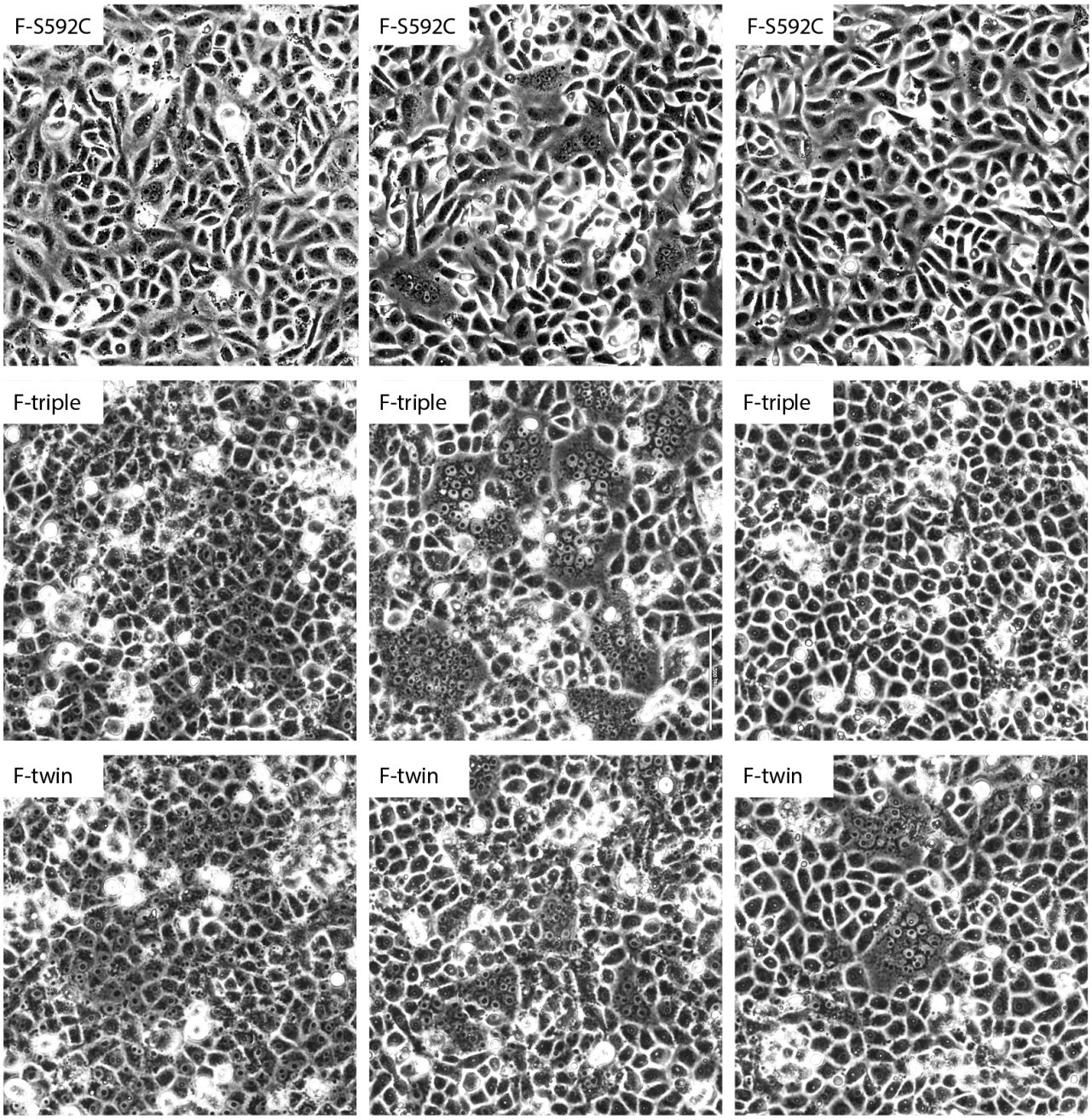
F-S592C
F-S592C
F-S592C
F-triple
F-triple
F-triple
F-twin
F-twin
F-twin
-DTT/-3G
+DTT/-3G
+DTT/+3G

# Figure 5

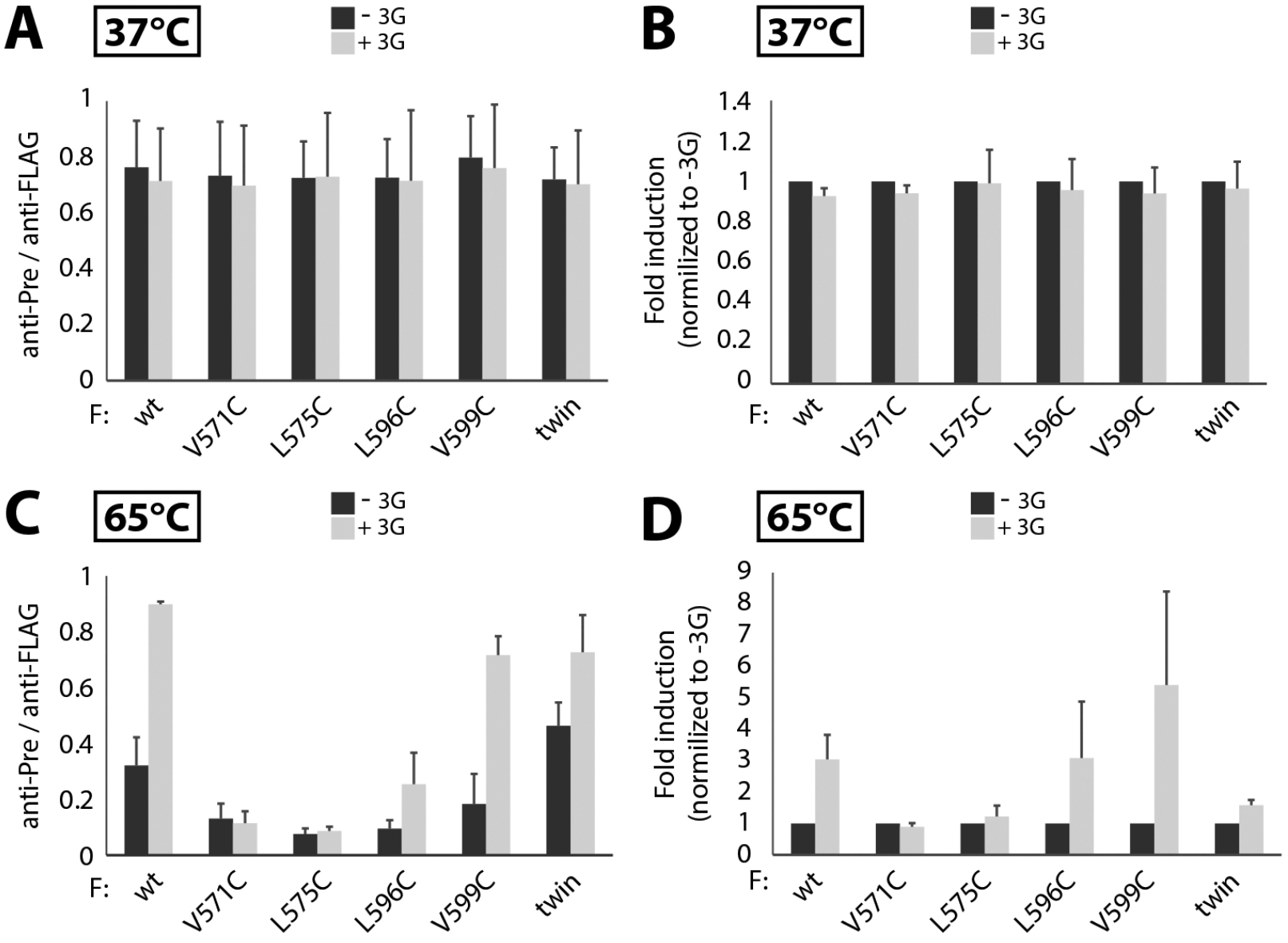
A
37°C
- 3G
+ 3G
anti-Pre / anti-FLAG
1
0.8
0.6
0.4
0.2
0
F:
wt
V571C
L575C
L596C
V599C
twin
B
37°C
- 3G
+ 3G
Fold induction
(normilized to -3G)
1.4
1.2
1
0.8
0.6
0.4
0.2
0
F:
wt
V571C
L575C
L596C
V599C
twin
C
65°C
- 3G
+ 3G
anti-Pre / anti-FLAG
1
0.8
0.6
0.4
0.2
0
F:
wt
V571C
L575C
L596C
V599C
twin
D
65°C
- 3G
+ 3G
Fold induction
(normilized to -3G)
9
8
7
6
5
4
3
2
1
0
F:
wt
V571C
L575C
L596C
V599C
twin

Figure 6

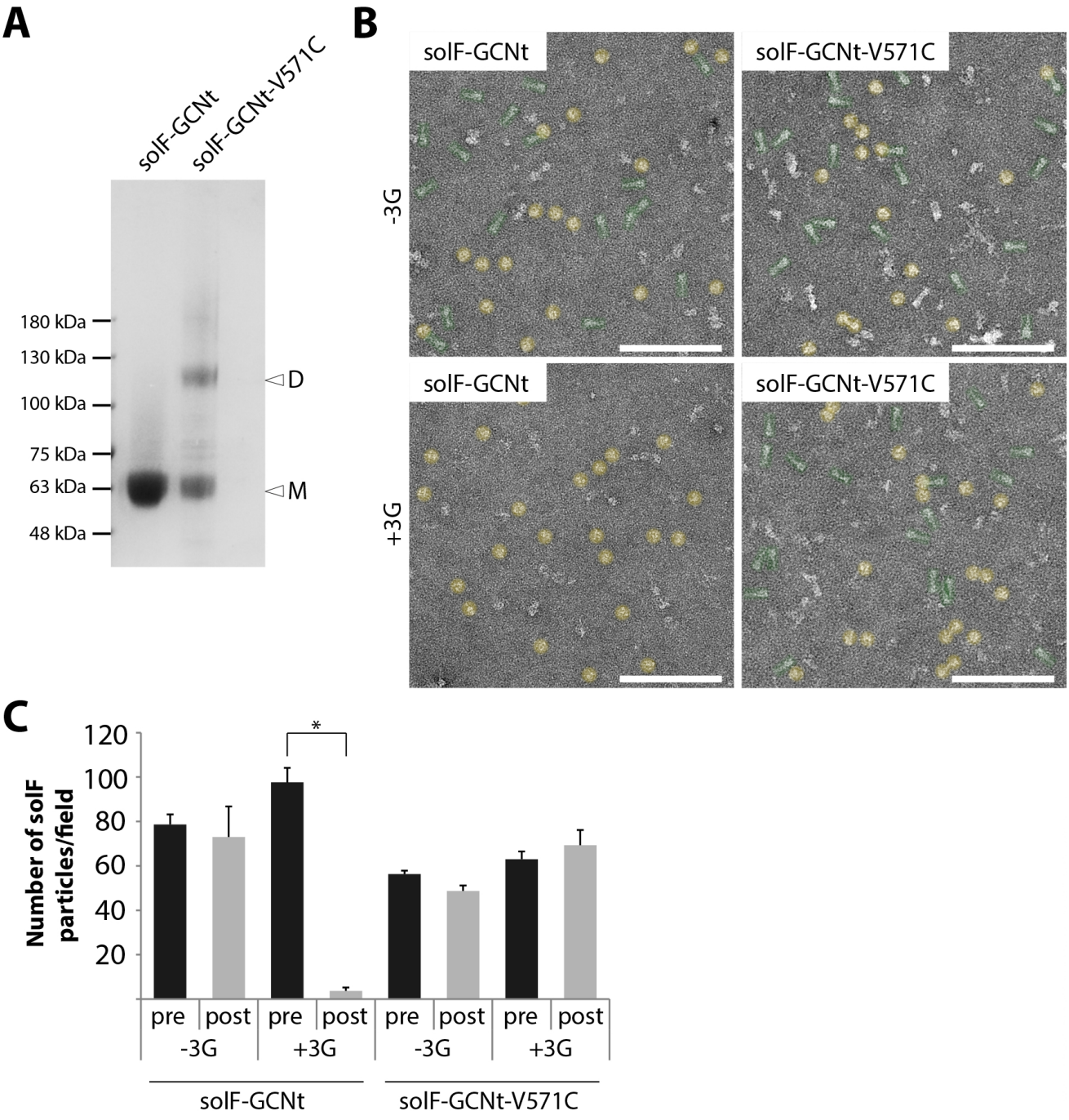
A
solF-GCNt
solF-GCNt-V571C
180 kDa
130 kDa
100 kDa
75 kDa
63 kDa
48 kDa
D
M
B
solF-GCNt
solF-GCNt-V571C
-3G
+3G
C
Number of solF particles/field
120
100
80
60
40
20
*
pre
post
pre
post
pre
post
pre
post
-3G
+3G
-3G
+3G
solF-GCNt
solF-GCNt-V571C

Figure 7

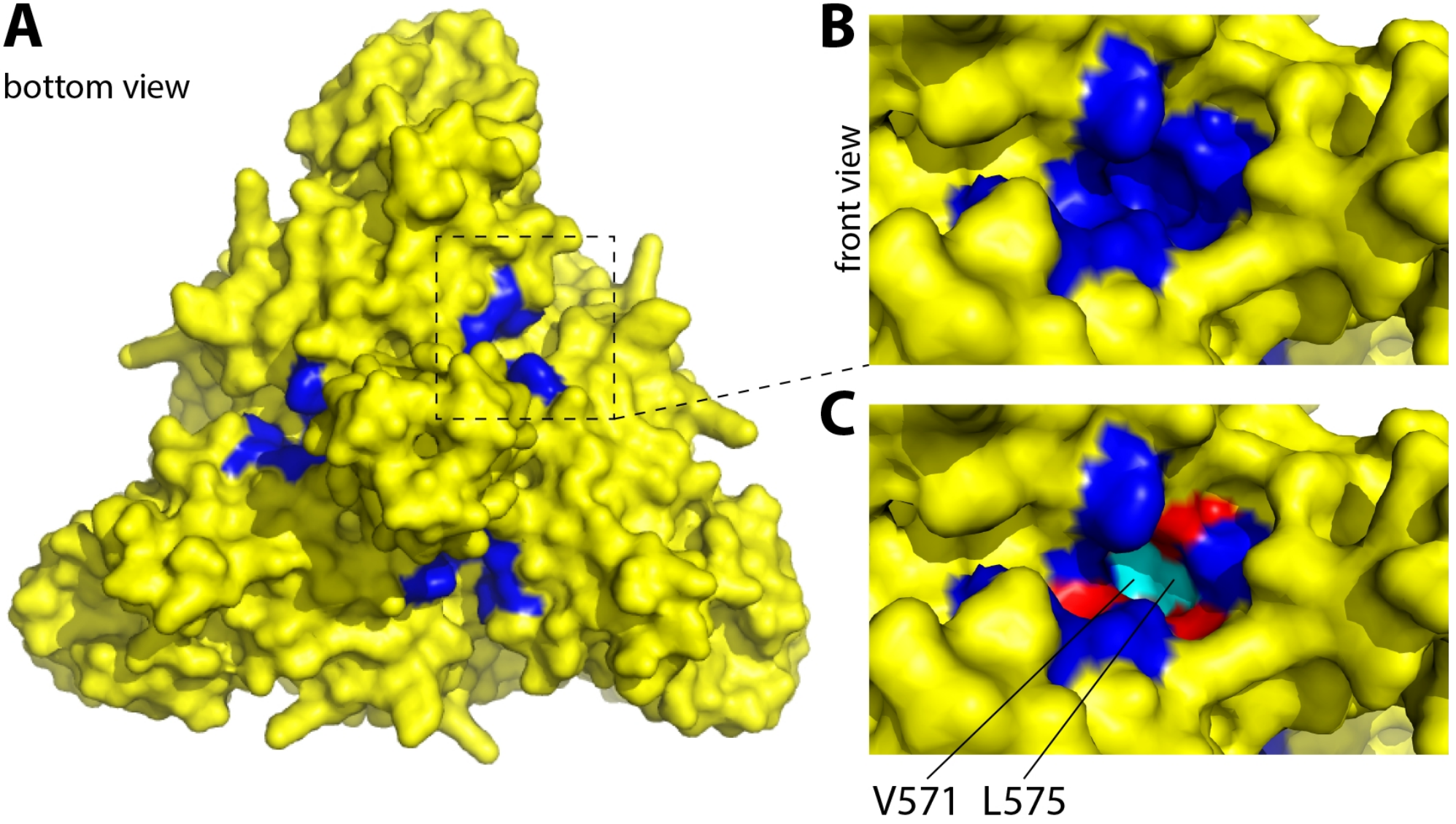

Figure 8

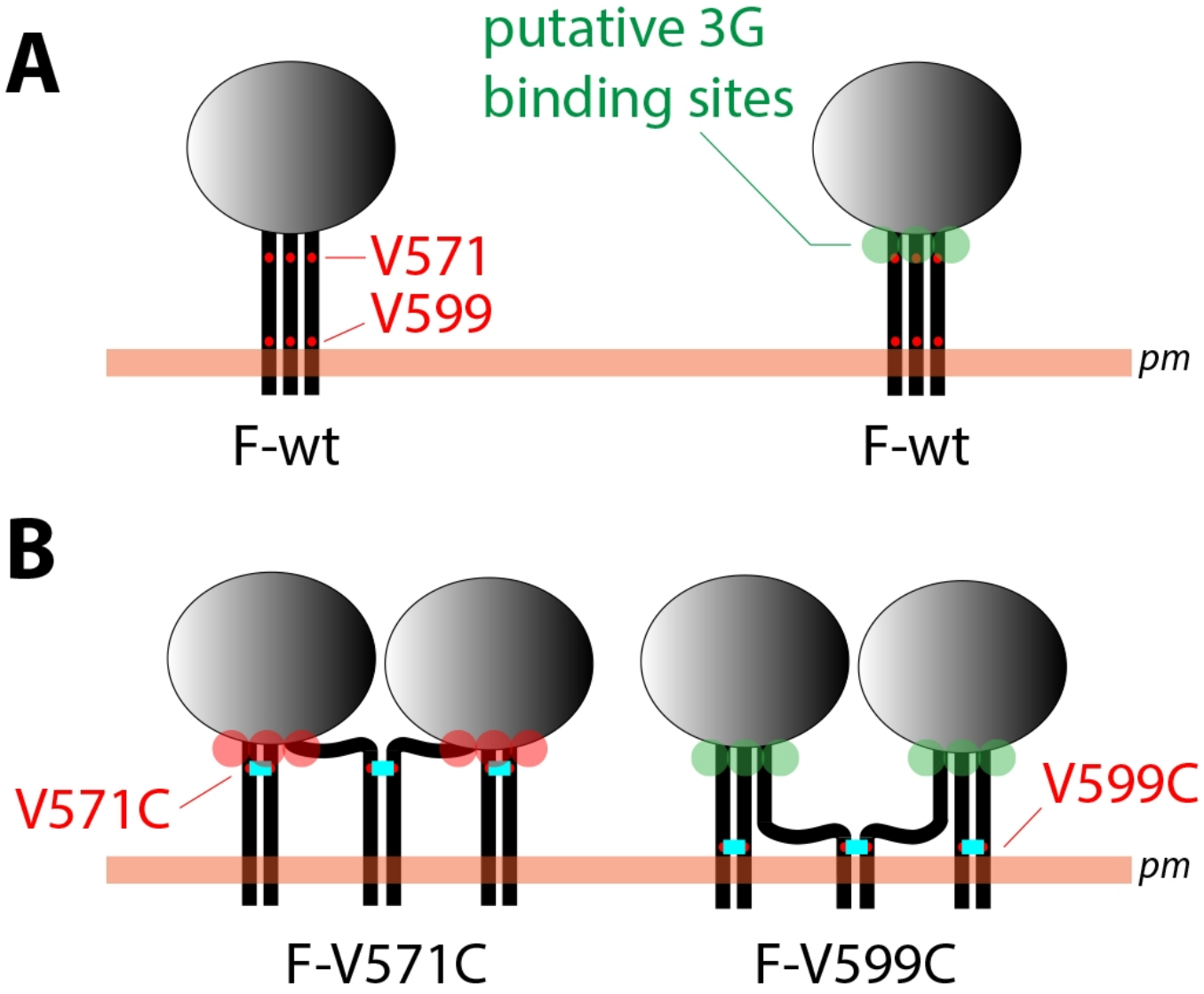
A
putative 3G
binding sites
V571
V599
pm
F-wt
F-wt
B
V571C
V599C
pm
F-V571C
F-V599C